NANO LETTERS

2006
Vol. 6, No. 7
1514−1517

Synthesis and Characterization of Phase-Change Nanowires

Stefan Meister,[†] Hailin Peng,[†] Kevin McIlwrath,[‡] Konrad Jarausch,[‡] Xiao Feng Zhang,[‡] and Yi Cui*,[†]

Department of Materials Science and Engineering, Stanford University, Stanford, California 94305, and Electron Microscope Division, Hitachi High Technologies America, Inc., 5100 Franklin Drive, Pleasanton, California 94588

Received May 15, 2006

ABSTRACT

Phase-change memory materials have stimulated a great deal of interest although the size-dependent behaviors have not been well studied due to the lack of method for producing their nanoscale structures. We report the synthesis and characterization of GeTe and Sb_2Te_3 phase-change nanowires via a vapor–liquid–solid growth mechanism. The as-grown GeTe nanowires have three different types of morphologies: single-crystalline straight and helical rhombohedral GeTe nanowires and amorphous curly GeO_2 nanowires. All the Sb_2Te_3 nanowires are single-crystalline.

The crystalline to amorphous phase change in chalcogenide alloy thin film materials accompanied with optical reflectivity and electrical resistivity changes has been exploited for data storage such as DVD and random access nonvolatile memory, respectively.[1−4] Recent studies on doped SbTe narrow lines fabricated by thin film deposition and lithography showed fast nanosecond and low-power switching and suggested that the nanowire (NW) geometry could be ideal for nonvolatile memory devices.[5] However, the size dependence of phase-change behavior has not been well studied due to the lack of method for producing their NW structures.

Over the last 10 years the vapor−liquid−solid (VLS) mechanism has been demonstrated to be a general method for producing one-dimensional IV, II−VI, and III−V semiconducting NWs.[6−12] Gold nanoparticles are often used as universal catalysts to define the growth of these materials into wirelike structures. Here we exploit the VLS growth of GeTe (GT) and Sb_2Te_3 (ST) phase-change NWs with Au nanoparticles as catalysts. The family of Ge−Sb−Te (GST) materials is one of the most important systems for phase-change memory devices due to their rapid reversible change between crystalline and amorphous states at temperatures compatible with those of device applications (for $Ge_2Sb_2Te_5$, melting point 610 °C, glass transition temperature 350 °C).[4] Germanium telluride and ST are the two important members of this family of materials and function as the basis to fabricate GST ternary alloys. They have melting points of 724 and 630 °C[13] and amorphous phase crystallization temperatures of 145[14] and 77 °C,[15] respectively. To investigate the fundamental possibility of a VLS growth with Au as the catalyst, we have looked into the phase diagrams of the materials involved. As shown in Figure 1A, GT and ST have a relatively simple bulk quasi-binary phase diagram with Au. The eutectic temperatures are at 480 and 454 °C,

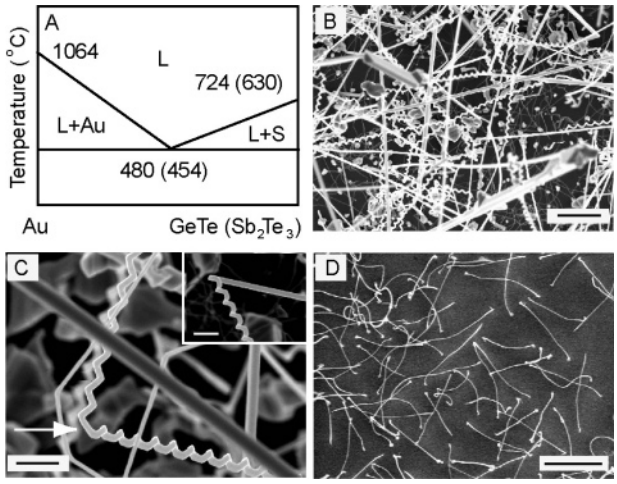

Figure 1. (A) Quasi-binary phase diagram between Au and GT or ST: L, liquid; S, solid. The drawing is not to scale but only meant for showing the temperature values and general shape of the diagram. (B) SEM image of as-grown NWs from GT evaporation with three types of morphologies; scale bar represents 2 μm. (C) High-resolution SEM image of the helical GT NWs with two different pitch sections. The white arrow indicates a pitch change point. Inset is a SEM image of straight-helical NW; scale bar represents 500 nm. (D) SEM image of thin and curly type III NWs from GT evaporation; scale bar represents 2 μm.

* To whom correspondence should be addressed. E-mail: yicui@stanford.edu.
[†] Stanford University.
[‡] Hitachi High Technologies America, Inc.

10.1021/nl061102b CCC: $33.50
Published on Web 06/17/2006

respectively.[13] The phase diagram suggests that it is possible to use Au nanoparticles for VLS growth of GT and ST phase-change NWs. Due to the small size of Au nanoparticles, the eutectic temperature might be lower than the bulk value.[16]

Nanowires were grown on silicon ⟨100⟩ substrates with a native oxide that were functionalized with 0.1% w/v aqueous poly-L-lysine solution (Ted Pella) and dipped into 50 nm diameter Au colloid solution (Ted Pella). The negatively charged Au nanoparticles stick to the positively charged poly-L-lysine. The substrates were placed downstream in a 1 in. diameter horizontal tube furnace (Lindberg/Blue M) with the source material, finely ground GT (Alfa Aesar, 99.999%) or ST (Alfa Aesar, 99%), placed in the hot center region. A 5% H_2 in N_2 gas mixture acted as a carrier gas to transport the vapor to the colder furnace region. Before each experiment, the quartz tube of the furnace was evacuated to <100 mTorr and flushed with the carrier gas repeatedly to decrease oxygen contamination. Germanium telluride NWs were grown at ∼50 Torr and ST NWs were grown at 1 atm pressure. Typical parameters for the NW synthesis were as follows: temperature $T = 450$ °C, duration time $t = 1-6$ h, and carrier gas flow rate = 150 sccm. Antimony telluride NWs grew preferentially within 10 cm of the hot center region of the furnace, where the temperature was ∼440 °C and the best GT NW growth was achieved in the colder region within 5−10 cm of the furnace end with a temperature of ∼370 °C. Samples were also grown on 50 nm thick Si_3N_4 membranes for further studies with a transmission electron microscope (TEM).

The NW surface morphologies were examined in an FEI Sirion scanning electron microscope. The morphologies and chemical compositions were also studied using a 200 kV Hitachi HD-2300 scanning transmission electron microscope (STEM) at Hitachi High Technologies America in Pleasanton, CA. The bright-field images were taken using a retractable phase contrast detector, and the *Z*-contrast images were received by a HAADF (high angle annular dark field) detector. A special design of the HD-2300 also allowed for obtaining nanodiffraction patterns using a 2 nm diameter electron beam simultaneously with the *Z*-contrast images. Chemical analysis was done using a high sensitivity energy-dispersive X-ray spectrometer (EDX, NORAN System). Quantitative point analysis as well as chemical mapping was performed. Atomic structures and crystalline orientations of the nanowires were studied using a 300 kV Hitachi H-9500 transmission electron microscope with a point resolution of 1.8 Å. High-resolution transmission electron microscopy (HRTEM) images were taken using a 2048 × 2048 pixel CCD camera. The NWs studied were those directly grown on the Si_3N_4 membranes or deposited onto carbon film supported by Cu grids. The specimen tilting in the microscope was less than 5° to reach a zone axis which reflected the growth orientations.

Figure 1B shows a typical scanning electron micrograph (SEM) of as grown NWs after GT powder evaporation. Three types of morphologies can be identified. The first type (type I) consists of long and straight NWs with diameters in the range of 50−200 nm and lengths up to tens of micrometers. Most interestingly, the second type (type II) is the helical structures with diameters of 50−200 nm and lengths up to tens of micrometers. The helical pitch is 200−400 nm. Type I and II NWs have a very similar diameter and length distribution. Higher magnification SEMs indicate that straight and helical structures can coexist in the same NWs as shown in the Figure 1C inset, suggesting that type I and II might have the same chemical composition and crystal structure. It is also noted that the helical NWs can change their pitch by having a sharp turn as shown by a white arrow in Figure 1C. A three-dimensional helical structure can also become a nearly two-dimensional zigzag structure. (Figure 1C). Both left- and right-handed helical NWs can be found with equal probability. These observations are not yet fully understood and further studies are needed. The third type (type III) consists of thin and curly NWs below type I and II and is mostly close to the substrate surface (Figure 1B). Type III has a narrow diameter distribution centered at ∼35 nm (Figure 1D), which is smaller than the size of 50 nm diameter Au nanoparticles (see the explanation below). The length is approximately several micrometers. Each type of NW accounts for a significant fraction of the final products.

To characterize the chemical compositions and structures, we have carried out EDX, HRTEM and electron diffraction (ED) studies. Type I and II NWs show the same chemical composition and crystal structure and are now discussed first. A dark field (*Z*-contrast) TEM image of a single straight-helical NW shows a uniform contrast along the NW (Figure 2A), suggesting relative uniform composition along the NW. The brighter contrast at the end of the NW indicates a large atomic number and that it is indeed a gold nanoparticle catalyst (Figure 2A, inset). The presence of a Au nanoparticle at the end of a NW is reminiscent of a VLS growth mechanism. The broad diameter distribution of 50−200 nm in our NWs can be attributed to the sidewall coating during growth. The size of Au nanoparticles and the growth conditions including gas pressure and temperature can be used to control the NW size in the future. Elemental mapping on single NWs with EDX was carried out to study the spatial distribution of chemical compositions. The probe size of 2 nm in STEM gives a high spatial resolution. Figure 2B is a STEM image of a NW and parts C and D of Figure 2 show the spatial distribution of the Ge and Te element on the same NW. The quantitative analysis determined an atomic percentage of 51% and 49% for Ge and Te, respectively. This indicates that the chemical composition for type I and II NWs is GeTe. The spatial mapping of EDX also suggests that the distribution of Ge and Te is uniform throughout the whole NW and there is no significant local chemical composition variation within the instrumental error.

The HRTEM studies on single type I straight NWs (Figure 2E) clearly shows the lattice planes with a spacing of 2.15 Å, consistent with the (024) lattice planes of the rhombohedral GeTe crystal structure and confirm that type I NWs are single-crystalline. HRTEM studies also indicate that there is no significant oxide layer (<1 nm) on the NW surface, which is important information for making electrical contacts

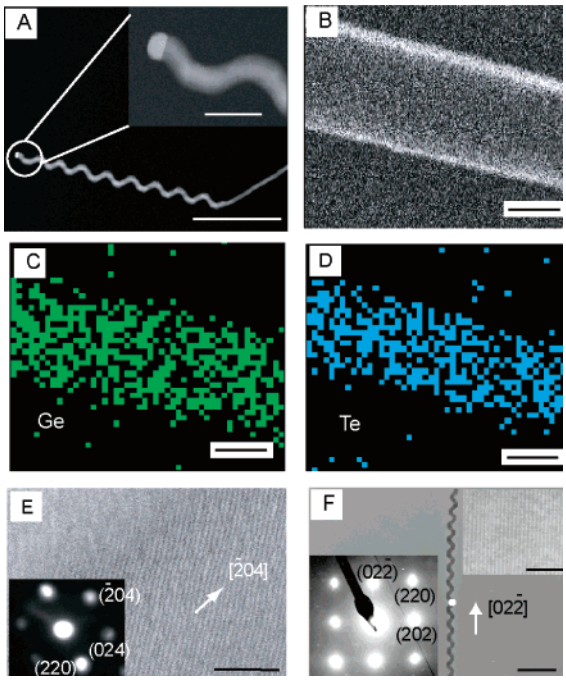

Figure 2. (A) *Z*-contrast TEM image of a straight-helical GT NW. The bright spot at the tip corresponds to a high-*Z* element gold nanoparticle; scale bar represents 1 μm. Inset shows a higher magnification *Z*-contrast image of the Au tip; scale bar represents 150 nm. (B) STEM image of a GT NW. (C and D) EDX elemental mapping of Ge (green) and Te (blue) on the same part of the GT NW as shown in part B. Scale bars in parts B to D represent 100 nm. (E) HRTEM image of a single crystalline rhombohedral GT NW. The lattice (024) plane with a spacing of 2.15 Å is shown. The NW growth direction is indicated by the white arrow perpendicular to the lattice plane (−204); scale bar represents 3 nm. Inset shows a nano-ED pattern taken on the same NW. (F) Low-magnification TEM image of a helical GT nanowire. A white spot marks the location for HRTEM (top inset) and ED (bottom inset); scale bars represent 1 μm (main panel) and 3 nm (top inset).

in the future nonvolatile memory switching studies. The nano-ED of the same NW shows regular spot patterns (Figure 2E inset), which also confirms the single crystalline nature of the NWs. The diffraction spots in the ED patterns can be indexed, and the growth direction of NWs is along [−102] or [102] direction (perpendicular to the (−204) or (204) lattice planes). The HRTEM (Figure 2F top inset) and ED (Figure 2F bottom inset) data taken at the same position (Figure 2F white spot) of a type II helical NW also indicate that they are single-crystalline rhombohedral GeTe. The visible lattice planes in the Figure 2F inset are (202) with a spacing of 2.98 Å. The growth direction of helical NWs is [01−1] or [011] (perpendicular to (02−2) or (022) lattice planes).

For type III NWs, low-magnification TEM images (Figure 3A) show the thin and curly NWs with black contrast at the tip. A *Z*-contrast image (Figure 3A inset) indicates that the tip has an element of higher atomic number than the NWs, corresponding to a Au nanoparticle. This suggests the growth is via a VLS mechanism. Type III NWs are not stable under an electron beam. The focused electron beam can drill holes into the NWs within several seconds as shown in Figure 3B. This opens up a possibility in the future to engineer the

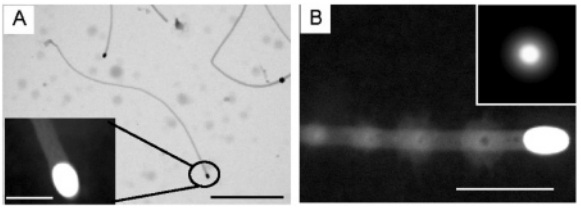

Figure 3. (A) Low-magnification TEM image on type III NWs (GeO_2). The black spots at the end of the NWs correspond to the Au nanoparticles; scale bar represents 800 nm. Inset shows a high-magnification *Z*-contrast TEM image on a selected NW tip. The Au nanoparticle at the tip shows a bright contrast. Scale bar represents 80 nm. (B) *Z*-contrast TEM image of a GeO_2 NW with four drilled holes using an electron beam; scale bar represents 150 nm. Inset shows an ED pattern showing the amorphous nature of GeO_2 NW.

structure of these NWs by electron beam. The nano-ED (Figure 3B inset) shows neither ring nor spot patterns suggesting the NWs are amorphous. The EDX spectra of NWs show Ge and O signals without detectable Te. The atomic ratio of Ge to O is calculated to ∼2 (Figure S1 in Supporting Information). These suggest that type III NWs are amorphous GeO_2. The mean NW diameter at ∼35 nm, which is smaller than the initial Au nanoparticle size, might be due to the wetting properties between Au and GeO_2. The interface between the Au and NWs is curvy (Figure 3A inset and Figure 3B) rather than flat as in type I and II NWs (Figure 2A and inset). This changes the shape of Au nanoparticle from nearly spherical into elliptical. The NW dimension is controlled by the short axis of the Au and thus is smaller than the initial Au size. The dependence of interface curvature on the materials is currently under investigation.

We attribute the existence of both single crystalline GeTe NWs and amorphous GeO_2 NWs to the O_2 residue in our growth system. When the synthesis started, GeO_2 NWs grew first due to the initial high concentration of O_2. This speculation was supported by the fact that GeO_2 NWs were found in areas closest to the substrate surface. Oxidation after NWs were taken out of the growth tube was less likely to cause the whole NW to become GeO_2 since HRTEM studies do not show a significant oxide layer on type I and II single crystalline NWs. However, we cannot rule out the possibility that GeO_2 NWs were chemically transformed from GeTe NWs by oxidation during the growth at high temperature. After the O_2 level was reduced by forming GeO_2 NWs, GeTe nanowires started to nucleate and grow and stay above GeO_2 NWs.

We also developed the VLS growth method for ST NWs. Figure 4A shows a typical SEM image of as-grown ST NWs on a substrate surface and the inset is a high-resolution SEM image (Figure 4A inset) showing Au nanoparticles at the tip of NWs. The images suggest that the growth is most likely through the VLS mechanism. Antimony telluride NWs have lengths up to ∼1 μm. Nanowires grown from the 50 nm diameter Au nanoparticles have a larger mean diameter of ∼70 nm. After the growth, the diameter of the Au nanoparticles increases to ∼100 nm. The EDX elemental mappings of a single ST NWs are shown in Figure 4C−F. Antimony

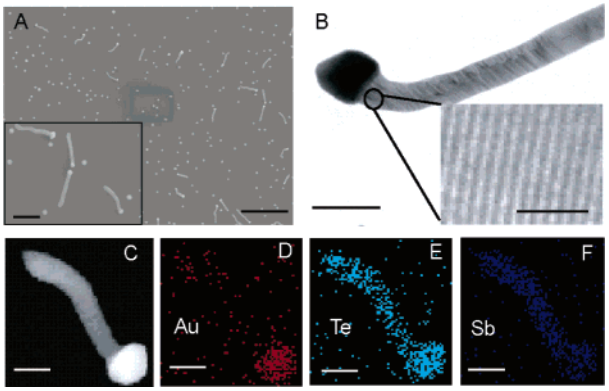

Figure 4. (A) Low-magnification SEM image of as-grown ST NW; scale bar represents 2 μm. Inset shows a high-magnification SEM image of as-grown ST NWs. The bright spots at the tip correspond to Au nanoparticles; scale bar represents 500 nm. (B) TEM image of a ST NW. The black spot at the tip is Au. Scale bar represents 200 nm. Inset shows a HRTEM on the same NW with a 3.33 Å *d* spacing corresponding to (104) planes of the rhombohedral ST; scale bar represents 2 nm. (C) *Z*-contrast image of a ST NW. The white particle at the tip is Au. (D−F) The EDX elemental mappings for Au, Te, and Sb, respectively. Scale bars represent 100 nm in parts C−F.

and Te are distributed uniformly throughout the whole NWs including inside the Au nanoparticle at the tip. This suggests that Sb and Te have significant solubility in Au nanoparticles. After the NW growth, the Au nanoparticles were alloyed to form Au−Sb−Te, causing the volume increase. Transmission electron microscopy studies (Figure 4B) confirm that Au nanoparticles are at the end of the NW tips. High-resolution TEM (Figure 4B inset) shows the ST NWs are single crystalline. The measured lattice spacing of 3.33 Å corresponds to the *d* spacing of the (104) planes of the rhombohedral ST.

In summary, we have successfully synthesized single crystalline GT straight and helical NWs and ST NWs via a VLS mechanism. Germanium oxide NWs can also be produced due to the presence of an oxygen residue during growth. The success in synthesizing these phase-change NWs opens up the opportunity for studying the size and surface dependence of crystalline−amorphous phase transformation.

Acknowledgment. We thank Dr. Richard Chin for help with TEM and Professor Philip Wong for helpful discussion. Y.C. acknowledges the financial support from Stanford CIS seed fund.

Supporting Information Available: EDX spectrum of a single amorphous GeO_2 nanowire. This material is available free of charge via the Internet at http://pubs.acs.org.

References

(1) Ovshinsky, S. R. *Phys. Rev. Lett.* **1968**, *21*, 1450.
(2) Feinleib, J.; de Neufville, J.; Moss, S.C.; Ovshinsky, S. R. *Appl. Phys. Lett.* **1971**, *18*, 254.
(3) Adler, D.; Henisch, H. K.; Mott, N. *Rev. Mod. Phys.* **1978**, *50*, 209.
(4) Hudgens, S.; Johnson, B. *MRS Bull.* **2004**, *11*, 829.
(5) Lankhorst, M. H. R.; Ketelaars, B. W. S. M. M.; Wolters, R. A. M. *Nat. Mater.* **2005**, *4*, 347.
(6) Wagner, R. S.; Ellis, W. C. *Appl. Phys. Lett.* **1964**, *4*, 89.
(7) Morales, A. M.; Lieber, C. M. *Science* **1998**, *279*, 208.
(8) Wu, Y.; Yang, P. *Chem. Mater.* **2000**, *12*, 605.
(9) Duan, X.; Lieber, C. M. *Adv. Mater.* **2000**, *12*, 298.
(10) Duan, X.; Lieber, C. M. *J. Am. Chem. Soc.* **2000**, *122*, 188.
(11) Björk, M. T.; Ohlsson, B. J.; Sass, T.; Persson, A. I.; Thelander, C.; Magnusson, M. H.; Deppert, K.; Wallenberg, L. R.; Samuelson, L. *Appl. Phys. Lett.* **2002**, *80*, 1058.
(12) Kuykendall, T.; Pauzauskie, P. J.; Zhang, Y.; Goldberger, J.; Sirbuly, D.; Denlinger, J.; Yang, P. *Nat. Mater.* **2004**, *3*, 528.
(13) Prince, A.; Raynor, G. V.; Evans, D. S. *Phase Diagrams of Ternary Gold Alloys*: Institute of Metals: Brookfield, VT, 1990.
(14) Yamada, N.; Ohno, E.; Nishiuchi, K.; Akahira, N. *J. Appl. Phys.* **1991**, *69*, 2849.
(15) Damodara Das, V.; Soundararajan, N.; Pattabi, M. *J. Mater. Sci.* **1987**, *22*, 3522.
(16) Zhang, Z.; Li, J. C.; Jiang, Q. *J. Phys. D*: *Appl. Phys.* **2000**, *33*, 2653.

NL061102B